Heliyon 9 (2023) e17732

Contents lists available at ScienceDirect

Heliyon

journal homepage: www.cell.com/heliyon

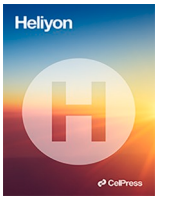

Albumin-coated copper nanoparticles for photothermal cancer therapy: Synthesis and in vitro characterization

Reeju Amatya [a], Donghee Lee [a], Marium Sultana [a], Kyoung Ah Min [b,**], Meong Cheol Shin [a,*]

[a] College of Pharmacy and Research Institute of Pharmaceutical Sciences, Gyeongsang National University, 501 Jinju Daero, Jinju, Gyeongnam, 52828, Republic of Korea

[b] College of Pharmacy and Inje Institute of Pharmaceutical Sciences and Research, Inje University, 197 Injero, Gimhae, Gyeongnam, 50834, Republic of Korea

ARTICLE INFO

Keywords:
Albumin
Copper
Nanoparticle
Cancer
Photothermal therapy

ABSTRACT

Copper nanoparticles (CuNPs) have attracted great interest in various biomedical research fields due to their superior optical and plasmonic properties. In the present study, we synthesized bovine serum albumin (BSA)-coated CuNPs (BSA-CuNPs) by adopting the aqueous reduction method in 2-step procedures. The prepared BSA-CuNPs were characterized in vitro for their physical characteristics and photothermal activity. The successful synthesis of BSA-CuNPs was verified through transmission electron microscopy (TEM), field emission scanning electron microscopy (FE-SEM), dynamic light scattering (DLS), differential scanning calorimetry (DSC), X-ray diffraction (XRD), Fourier transform infrared (FT-IR) spectroscopy, and ultraviolet–visible (UV-VIS) light spectroscopy. The prepared BSA-CuNPs revealed a great light-to-heat conversion capacity and good photothermal stability. Notably, accompanied by laser irradiation, the BSA-CuNPs elicited significantly higher cytotoxicity on tumor cells than the control group. Preliminary animal studies to determine the biosafety and pharmacokinetics (PK) profiles exhibited that the BSA-CuNPs have a maximum tolerable dose (MTD) of 16 mgCu/kg and a relatively long plasma half-life of 1.98 h. Overall, our findings demonstrated that BSA-CuNPs might be a potential photothermal therapeutic agent for cancer treatment.

1. Introduction

Nanotechnology has attracted significant attention in many research fields, including cancer research. While many nanoparticles (NPs) are generally developed to serve as drug carriers, some of them could function as diagnostic agents or even therapeutics [1,2]. Recently, various metal NPs have been of particular interest due to their potential utility as theranostic agents [3–8]. This is mainly due to their unique physical properties, including tunable optical characteristics, magnetic susceptibility, and photothermal activity [8]. Besides their intrinsic properties, the relative ease and simplicity of the synthesis process allow for broader research applications of metal NPs [8].

Among various metal NPs, CuNPs have drawn great interest in various research fields, including energy, catalysis, and potential

* Corresponding author.
** Corresponding author.
E-mail addresses: minkahh@inje.ac.kr (K.A. Min), shinmc@gnu.ac.kr (M.C. Shin).

https://doi.org/10.1016/j.heliyon.2023.e17732
Received 24 March 2023; Received in revised form 10 June 2023; Accepted 27 June 2023
Available online 27 June 2023

medical applications [9]. Specifically, recent studies have reported superior anticancer activity of CuNPs [10]. In this regard, Zhang's group developed various CuNPs, including copper phosphide (CuP), CuS, and $Cu_{1,2}O$ NPs for cancer theranostics [11–13]. Major advantages of the CuNPs over other NPs include biodegradability, moderate toxicity, and plasmonic nature [14]. Specifically, due to the great light-to-heat conversion efficiency, the CuNPs have also been considered a promising photothermal therapeutic agent [13, 14].

According to accumulating reports, PTT could become an effective means of cancer therapy [15]. Based on the surface plasmon resonance effects, a group of metal NPs could convert the absorbed light (most frequently in near-infrared wavelengths) to heat, and, by localized heating of the tumor tissue above mid-40 °C, selective induction of tumor cell death is available [16]. Various cell death mechanisms (e.g., apoptosis, necrosis, and necroptosis) were found to be involved with the photothermal effects [17]. The significant merits of this treatment approach are its effectiveness, less invasiveness, and safety [18]. Recent advances in cancer light therapy include the development of combination therapies of chemodynamic-photothermal [19], photodynamic-photothermal [20], chemo-photodynamic [21], and even chemo-chemodynamic-photothermal triple therapies [22]. Furthermore, there have also been studies to overcome the tissue penetration issues which limit the use of PTT in deep tissue tumors. An effective way to tackle this obstacle may be to utilize PTT agents that could function with light in the NIR-II region (1000–1700 nm) than the general NIR-I reigon (700–1000 nm) [23].

Because of the hydrophobicity of metal elements, metal NPs generally require a hydrophilic coating to ensure stability in the dispersion [24]. In this regard, various coating materials have been used. Among them, albumin has been widely adopted [25,26]. As an NP coating material, albumin has distinct merits such as cost-effectiveness, relative ease of synthesis, good biodegradability and biocompatibility, long plasma half-life, and availability of efficient drug loading [27]. As the most abundant protein in the plasma, albumin is a natural transport protein for various molecules [27]. Of note, copper also tends to bind albumin spontaneously, which could often lead to aggregation [28]. Specifically, for the bovine serum albumin (BSA), the copper-binding site has been inferred to be the site II (subdomain IIIA) region [29].

To date, there have been reported various methods to synthesize CuNPs [30]. However, the procedures often required relatively high reaction temperatures or fusion of Cu with other metallic materials to improve particle stability. Hence, developing a simpler way to synthesize CuNPs in ambient conditions would be beneficial. In the present study, we developed BSA-CuNPs and explored their applicability for PTT in cancer therapy. The BSA-CuNPs were synthesized by a simple 2-step process involving the reduction of copper ions, and the prepared particles were evaluated for their physical characteristics, photothermal activity, and stability in vitro. Further, preliminary animal studies were conducted to assess the biosafety and the PK profiles of the BSA-CuNPs.

2. Materials and methods

2.1. Materials

Copper sulfate pentahydrate ($CuSO_4 \bullet 5H_2O$; shortly "$CuSO_4$") and sodium borohydride ($NaBH_4$) were purchased from Sigma Aldrich (St. Louis., MO, USA). BSA was obtained from Amresco (Solon, OH, USA). All chemicals were of analytical grade.

2.2. Synthesis of BSA-CuNPs

$CuSO_4$ (2 mg as Cu^{2+}) 5 mg and BSA 10 mg were separately dissolved in 10 mL of double distilled water (DDW). After preparation, the $CuSO_4$ and BSA solution were mixed, and then 400 μL of 1 M NaOH was added to the mixture to adjust the pH to 9. To the BSA/Cu^{2+} complex, 1 mg of $NaBH_4$ dissolved in 1 mL of DDW was added to reduce the Cu^{2+}. The synthesis reaction was continued for 30 min at room temperature with stirring at 1000 rpm. After the reaction, the particles were separated from the unreacted $CuSO_4$ and BSA using an ultra-centrifugal device (molecular weight cut-off: 100 kDa; Amicon® Ultra-15 centrifugal filter units, Merck Millipore, Darmstadt, Germany). The final BSA-CuNPs suspension was concentrated to 1 mL and stored in a refrigerator (4 °C) before use. The BSA and copper contents in the BSA-CuNPs were quantified by micro-Bradford protein assay and ICP-OES, respectively.

2.3. Physical characterization

The morphology, size, and elemental composition of BSA-CuNPs were examined by high-resolution TEM (HR-TEM; Tecnai TF30 ST, FEI Co., Hillsboro, OR, USA) with energy dispersive spectroscopy (EDS). In addition, the freeze-dried BSA-CuNPs were observed with field emission scanning electron microscopy (FE-SEM; S-4700, Hitachi, Tokyo, Japan). The hydrodynamic size and zeta potential of the particles were measured by DLS (Zetasizer Nano ZS, Malvern Panalytical Ltd., Malvern, UK). The crystallinity of NP cores was investigated by DSC (TA Instruments Q20 DSC, New Castle, DE, USA) and XRD (Bruker APEX2 diffractometer, Bruker, Billerica, MA, USA). The presence of BSA coating on the surface of BSA-CuNPs was determined using FT-IR spectroscopy (VERTEX 80v, Bruker, Billerica, MA, USA). The UV-VIS absorption spectra were acquired at 300–800 nm with Synergy H1 Hybrid Multi-Mode Reader (BioTek U.S., Winooski, VT, USA).

2.4. In vitro assessment of the photothermal activity of BSA-CuNPs

To assess the photothermal activity, $CuSO_4$, BSA/Cu^{2+} complex [pH adjusted to 9; a.k.a. BSA/Cu^{2+} (pH 9)] and BSA-CuNPs suspensions were prepared to 500 μL of the total volume in Eppendorf tubes. The samples were then irradiated with a diode laser (spot

size: 5 × 8 mm^2, MDL–III–885, Changchun New Industries Optoelectronics Tech Co. Ltd, Changchun, China) for 10 min, and the sample temperature was monitored with an infrared camera (FLIR Systems, E5, Boston, MA, USA). In the first study, the $CuSO_4$, BSA/Cu^{2+} (pH 9), and BSA-CuNPs suspensions were irradiated with a laser in a fixed concentration (400 μgCu/mL) and laser power (1.3 W). Then, for the BSA-CuNPs, the laser experiment was performed at varying concentrations (0–400 μgCu/mL) with fixed laser power (1 W) and in a fixed concentration (400 μgCu/mL) with differential laser powers (0.8–1.3 W). Finally, to assess the photothermal stability of the BSA-CuNPs, the particle suspension (400 μgCu/mL) was irradiated with the diode laser at 1 W for 3 cycles by a switch "on and off" mode ("on" for 10 min and "off" for 10 min for each cycle).

2.5. Stability test

To evaluate the inter-day stability (in 4 °C storage condition), the particle appearance, size, UV-VIS spectrum, and photothermal activity of the BSA-CuNPs were measured daily for 5 consecutive days. For laser treatment, the particle suspension (400 μgCu/mL) was irradiated with the diode laser at 1 W for 10 min. The sample temperature was monitored with an infrared camera (FLIR Systems).

2.6. Cell culture

U87 MG human glioblastoma, A431 human epidermoid squamous carcinoma, and B16F10 murine melanoma cells were cultured in Dulbecco's Modified Eagle Medium (DMEM) containing 10% FBS, 1% penicillin-streptomycin, and 1% antibiotic antimycotic. The cell culture was maintained in a humidified cell incubator at 37 °C with 5% CO_2.

2.7. Cellular analysis of the cytotoxicity and photothermal activity of BSA-CuNPs

The U87 MG, A431, and B16F10 cells were seeded in 96-well plates to a density of 5 × 10^3 cells/well and incubated overnight. After incubation, varying concentrations of BSA-CuNPs were added to the cells to the final concentration of 0–120 μgCu/mL. The cells were further incubated for 48 h, and the relative cell viability was measured by WST-1 assay, following the vendor's protocol (iNtRON Biotechnology, Daejeon, Republic of Korea).

The photothermal effects on the tumor cells were evaluated on B16F10 cells. The B16F10 cells were seeded in 96-well plates at the density of 5 × 103 cells/well and, after overnight incubation, were treated with BSA-CuNPs (120 μgCu/mL). The diode laser was irradiated to the wells for 10 min. Three laser powers (1, 1.2, and 1.3 W) were adopted to induce maximum well temperatures of approximately 40, 45, and 50 °C, respectively. After the treatment, the cells were washed twice with phosphate buffer saline (PBS) and incubated for 48 h in a cell incubator. The relative cell viability was measured using WST-1 assay. In addition, the cellular images were acquired using a microscope after treating trypan blue to visualize the dead cells.

2.8. Preliminary animal studies

The animal experiments were carried out following the National Institute of Health Guidelines on the Use of Laboratory Animals and the protocol approved by the Gyeongsang National University Institutional Animal Care and Use committee for animal research (*GNU-220519-M0048-01*). The maximum tolerable dose (MTD) study was carried out by i.v. injection of elevating doses of BSA-CuNPs to healthy C57BL/6 mice (20 ± 1.5 g) (N = 3) and observation of any occurrence of death for 24 h. The MTD was determined as the highest dose that does not cause death or symptoms of severe adverse effects. For the pharmacokinetic (PK) analysis, 5 healthy C57BL/6 mice were administered with indocyanine green (ICG)-loaded BSA-CuNPs (420 μg ICG/kg and 40 mg BSA/kg) via tail vein injection. The ICG loading was carried out by adding ICG to the BSA solution (10-fold higher molar ratio to the BSA) before mixing the BSA with $CuSO_4$ solution. The further procedures were identical to the protocol of BSA-CuNPs synthesis. Blood was collected from the mice at pre-determined time points (5 min, 1, 2, 4, 6, and 8 h post-administration). After centrifugation, the plasma samples were transferred to 96 well plates (adequate for fluorescence-based assay), and the plasma ICG levels were quantified using FOBI Fluorescence In Vivo Imaging System (NeoScience Co., Ltd., Seoul, Republic of Korea) with an NIR channel. The fluorescence intensities of the wells were analyzed using NEOimage software (NeoScience Co., Ltd.), and the particle concentration (shown as BSA concentration) was plotted against the time course. The PK profiles were analyzed adopting non-compartmental analysis using the Phoenix® WinNonlin® software (Certara LP. Princeton, NJ, USA). The PK parameters, such as the plasma half-life ($t_{1/2}$), the area under the curve (AUC), and mean residence time (MRT), were calculated.

2.9. Statistical analysis

All data are shown as mean ± standard error of the mean (SEM). The statistically significant differences among the groups were analyzed by 1-way ANOVA (adopting Tukey's multiple comparison test as the post hoc test). Any data yielding $p < 0.05$ were considered statistically significant.

3. Results and discussion

3.1. Synthesis and physical characterization of BSA-CuNPs

Metal-based NPs have drawn significant interest in the medical research field because of their various activities that include antimicrobial and anticancer activity [8,10]. These NPs could be synthesized by stabilizing the metal ions utilizing effective ligands (e.g., pyrimidine derivatives, piperidine derivatives, and nophen ligands, etc.) [31–34] or reducing them in the presence of hydrophilic coating materials [35]. Interestingly, some of these ligands could not only function as stabilizers but also be utilized for metal ion sensors [36]. Notably, with metal complexation, the ligands could provide enhanced anti-oxidant, anti-microbial, and anticancer effects [31,37–39]. To date, for the synthesis of CuNPs, various methods have been proposed. Among them, the aqueous solution reduction method has been the most widely adopted [40]. This method is characterized by simple, easy-to-operate procedures and good yield [40]. For efficient synthesis, the reduction reaction was generally performed at relatively high temperatures (above 60 °C) [9]. In addition, the CuNPs have frequently been prepared as fused or coated with other materials (e.g., iron oxide, SiO_2, TiO_2, SnO_2, etc.) to improve its stability against oxidation [9].

In the present study, using the aqueous solution reduction method, the BSA-CuNPs were synthesized in two steps at room temperature. In the first step, the BSA/Cu^{2+} complex was prepared by mixing BSA and $CuSO_4$. As previously reported, the albumin and Cu^{2+} bound to each other, and, as shown in Figure S1A, the mixture solution appeared pale bluish and turbid [28,29,41]. Due to the acidity of the $CuSO_4$ solution, the pH of the mixture was about 5.6. Leaving the mixture at room temperature, sunken precipitates were observed. However, when the pH was adjusted to 9 by adding 1 M NaOH, the solution turned clear (Figure S1A available in the supplementary material), and the average hydrodynamic size of the BSA/Cu^{2+} was 265 nm. However, the BSA/Cu^{2+} could not maintain the nanometer size when changed the solution pH from 9 to 7. The solution became turbid again, and aggregation was apparent (data not shown). Therefore, in the 2nd step, $NaBH_4$, the reducing agent, was added to the BSA/Cu^{2+} (pH 9). Immediately, the solution color changed to wine red, suggesting the successful synthesis of BSA-CuNPs (Figure S1B available in the supplementary material). A major significance of the successful synthesis of BSA-CuNPs at ambient temperature may lie in the possibility of preparing CuNPs with a coating of therapeutic proteins instead of the BSA. The BSA-CuNPs were concentrated to 1 mL using the ultracentrifugal device (membrane pore size: 100 kDa) and stored in a 4 °C refrigerator until further use. The final BSA-CuNPs contained an average of

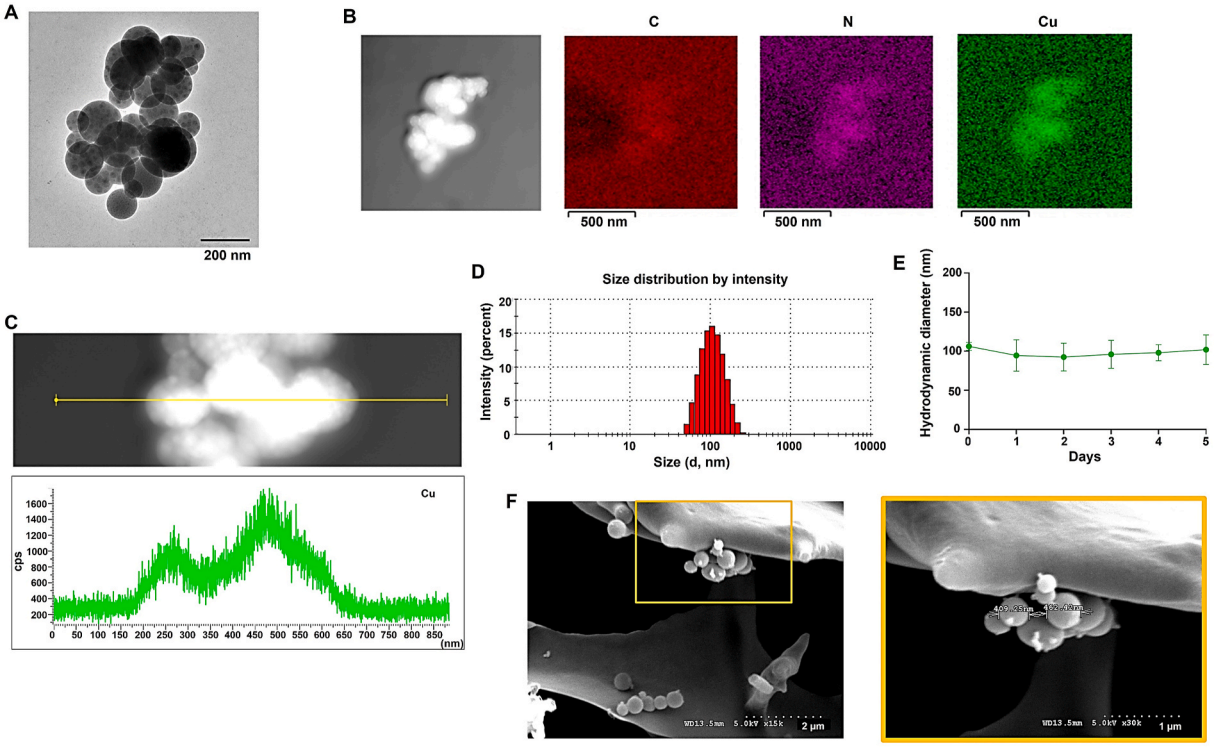

Fig. 1. Physical characterization of BSA-CuNPs. (A) High-resolution transmission electron microscopic (HR-TEM) images of BSA-CuNPs. (B) EDS analysis of BSA-CuNPs. The images from left to right are the scanning transmission electron microscopic (STEM) image of the particles and elemental distribution of carbon (C), nitrogen (N), and copper (Cu). (C) Enlarged STEM image of BSA-CuNPs and the spatial distribution of Cu. (D) Hydrodynamic size distribution of BSA-CuNPs. (E) Size stability of BSA-CuNPs. (F) Scanning electron microscopic (SEM) images of freeze-dried BSA-CuNPs. (BSA-CuNPs: bovine serum albumin-coated copper nanoparticles, EDS: energy dispersive spectroscopy, $CuSO_4$: $CuSO_4{\cdot}5H_2O$, and BSA/Cu^{2+}: BSA and Cu^{2+} complex)

410 μgCu and 8.2 mg of BSA.

The BSA-CuNPs were observed as clusters of spheres composed of multi-domain Cu core surrounded with BSA shells from the TEM image (Fig. 1A). The EDS results showed the presence of traceable amounts of N and Cu in the particle regions, suggesting the incorporation of BSA and Cu in the BSA-CuNPs (Fig. 1B). Furthermore, the spatial distribution of the Cu in the EDS result was in good accordance with the particle region on the yellow line shown in the scanning transmission electron microscope (STEM) image (Fig. 1C). As shown in Fig. 1D and E, the average hydrodynamic size of the BSA-CuNPs was 93.5(±9) nm (PDI: 0.13), and, when stored in a 4 °C refrigerator, the particles could maintain their size for 5 days without apparent aggregation. These results confirmed the size stability of the particle suspension at storage conditions. The average zeta potential was −10.9(±5.5) mV, presumably due to the negatively charged BSA corona of the particles. The SEM image of the freeze-dried BSA-CuNPs revealed clusters of globular-shaped particles, consistent with the TEM results (Fig. 1F). However, the average particle size was increased to about 400 nm (Fig. 1F).

The crystallinity of the Cu in the BSA-CuNPs was investigated by DSC and XRD. As seen from Fig. 2A, compared to the $CuSO_4$ with an obvious endothermic peak at around its melting point (110 °C), the BSA-CuNPs showed no distinct peaks, similar to the BSA [42]. Consistently, the XRD data evidenced the crystalline structure of the $CuSO_4$ [43], but both the BSA-CuNPs and BSA appeared amorphous (Fig. 2B). These results were in good accordance with Hadinejad et al. [42]. We further performed FT-IR spectroscopy. As shown in Fig. 2C, characteristic peaks of BSA at 1644 (1640) and 1531 (1541) cm^{-1} attributed to the amide I and II bands were clearly observed from the spectrum of BSA-CuNPs, suggesting the presence of BSA on the surface of the particles [44]. These results were in good accordance with the previously reported FT-IR data of the BSA-coated silver NPs [26].

The UV-VIS spectra of $CuSO_4$, BSA/Cu^{2+} (pH 9), and BSA-CuNPs suspensions were compared (Fig. 3). As can be seen in Fig. 3A, the $CuSO_4$ showed low intensity throughout 300–800 nm. In comparison, both the BSA/Cu^{2+} (pH 9) and BSA-CuNPs showed a concentration-dependent increase in intensity (Fig. 3B and C). Of note, the BSA-CuNPs exhibited an even higher increase in intensity than the BSA/Cu^{2+} (pH 9) (Fig. 3D). However, there was no distinct peak observed representative of the particle.

3.2. *In vitro assessment of the photothermal activity of BSA-CuNPs*

According to Sharma et al., CuNP is plasmonic and can convert the absorbed light to heat [8]. The SPR interband transition of the CuNP is known to occur at around 550–600 nm, close to the edge of the NIR-I wavelength [45,46]. Therefore, we evaluated the photothermal activity of the BSA-CuNPs using a 690 nm wavelength laser as compared with the $CuSO_4$ and BSA/Cu^{2+} (pH 9). The results are summarized in Fig. 3. All tested samples induced heat by laser irradiation (Fig. 4A). The samples' temperature initially rapidly increased with laser irradiation and gradually reached a plateau. Compared with the $CuSO_4$, a higher temperature rise was observed from the BSA/Cu^{2+} (pH 9) and the BSA-CuNPs. However, the BSA-CuNPs showed the highest temperature rise in the same concentration (400 μgCu/mL) and laser power (1.3 W).

The heat induction by the laser irradiation of BSA-CuNPs suspension correlated well with the BSA-CuNPs concentration and the laser power (Fig. 4B and C). In line with our expectation, the higher maximum temperature was observed at a higher concentration of BSA-CuNPs (29.5–49.8 °C at 50–400 μgCu/mL with 1 W laser power) and at a higher laser power (36.5–58.8 °C at 0.8–1.3 W with 400 μgCu/mL of BSA-CuNPs). To verify the photothermal stability of the particles, the BSA-CuNPs were irradiated with the laser by 3 cycles of a switch "on-and-off" mode. As shown in Fig. 4D, a similar maximum temperature level was observed for every cycle, evidencing the good photostability of the BSA-CuNPs. Compared with small molecule-based photosensitizers such as ICG, this good photostability has been recognized as a significant advantage of plasmonic metal NPs [47]. The results confirmed that this could also be the case for CuNPs.

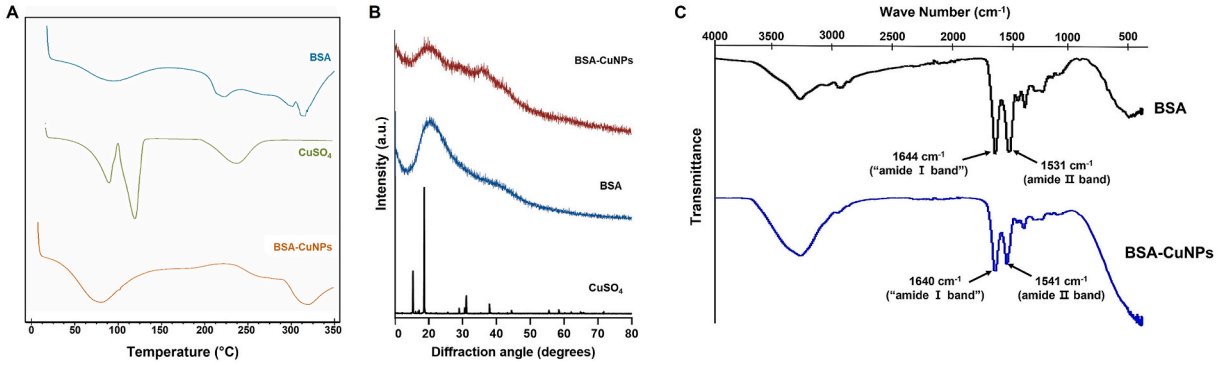

Fig. 2. Phase and FT-IR analysis of BSA-CuNPs. (A) Diffraction scanning calorimetry (DSC) data of BSA-CuNPs. (B) X-ray diffraction (XRD) results of BSA-CuNPs. (C) Fourier transform infrared (FT-IR) spectroscopic profiles of BSA-CuNPs. Both the DSC and XRD results indicated a structurally amorphous state of Cu in the particles, different from the $CuSO_4$. The characteristic peaks of BSA were identified from the FT-IR spectrum of BSA-CuNPs (at 1541 and 1640 cm^{-1}); suggesting the presence of BSA in the particles. (BSA-CuNPs: bovine serum albumin-coated copper nanoparticles, $CuSO_4$: $CuSO_4{\cdot}5H_2O$)

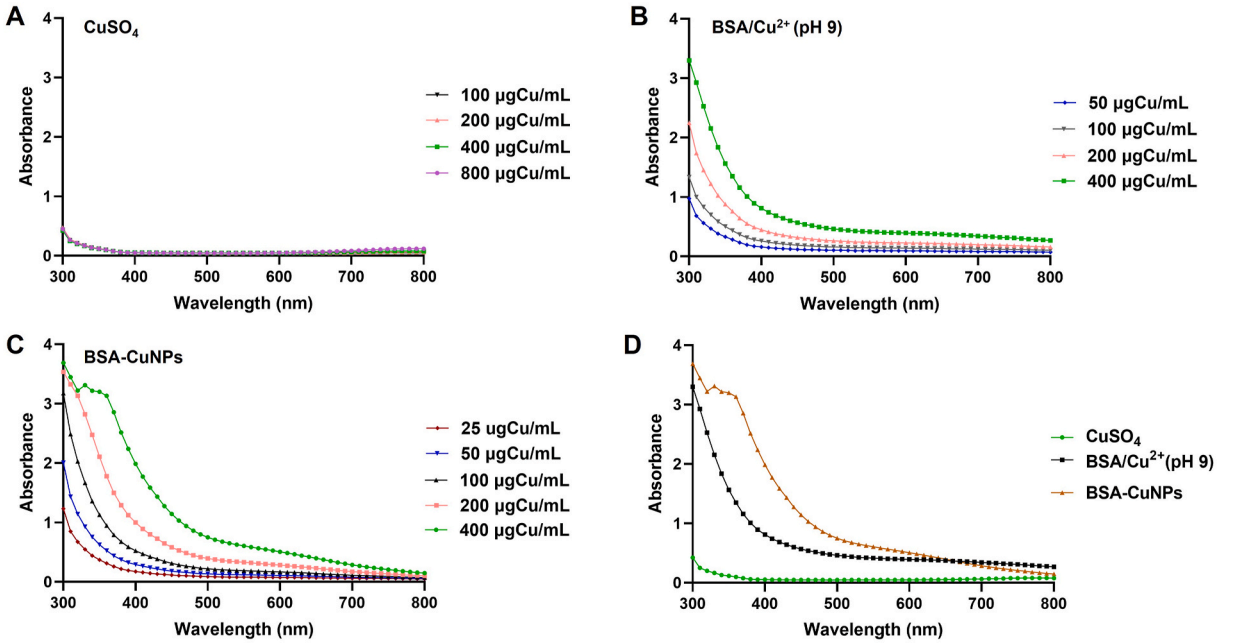

Fig. 3. The UV-VIS spectrometric analysis of BSA-CuNPs. The UV-VIS spectrum of (A) $CuSO_4$, (B) BSA/Cu^{2+} (pH 9), and (C) BSA-CuNPs. (D) Comparison of the UV-VIS spectrum of $CuSO_4$, BSA/Cu^{2+} (pH 9), and BSA-CuNPs in identical Cu concentrations. (BSA-CuNPs: bovine serum albumin-coated copper nanoparticles, $CuSO_4$: $CuSO_4{\cdot}5H_2O$, and BSA/Cu^{2+} (pH 9): BSA and Cu^{2+} complex present at pH 9 solution)

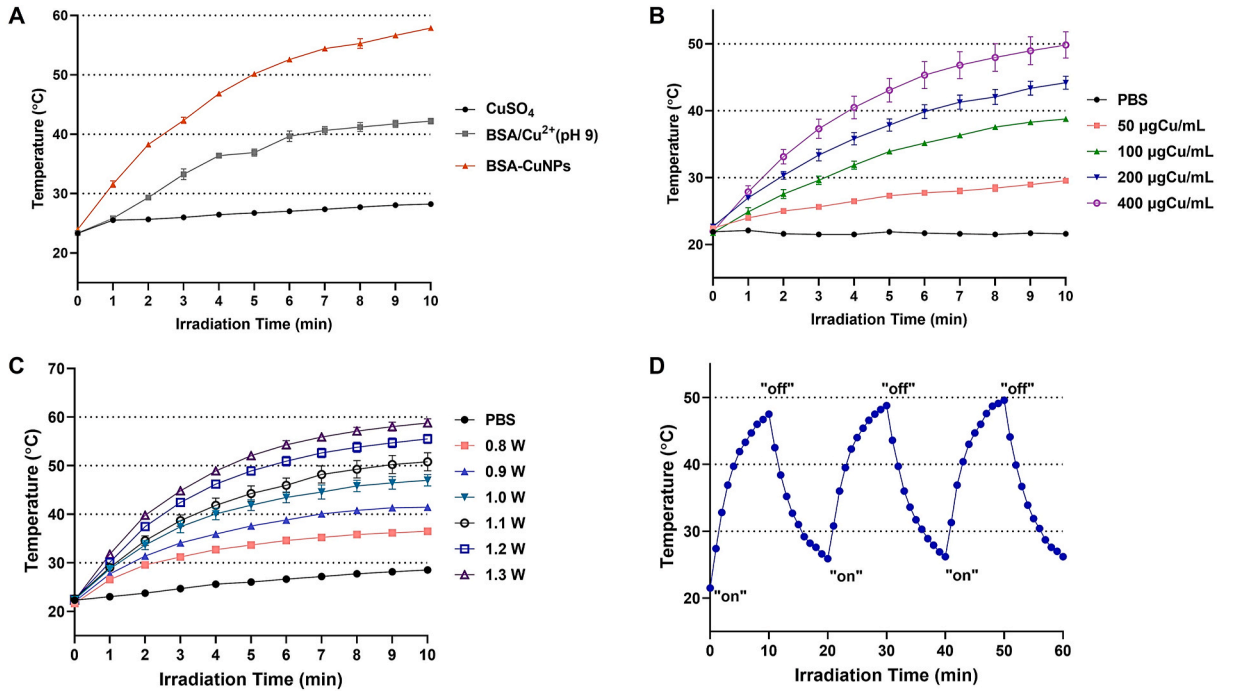

Fig. 4. *In vitro* evaluation of the photothermal activity of BSA-CuNPs. (A) Comparison of the temperature rise profiles of $CuSO_4$, BSA/Cu^{2+} (pH 9), and BSA-CuNPs. Temperature profiles of BSA-CuNPs with laser irradiation in (B) different particle concentrations (0–400 µgCu/mL) and (C) different laser powers (0–1.3 W). (D) Photothermal stability of BSA-CuNPs assessed with laser irradiation for 3 repetitive cycles of a switch "on" and "off". (BSA-CuNPs: bovine serum albumin-coated copper nanoparticles, $CuSO_4$: $CuSO_4{\cdot}5H_2O$, and BSA/Cu^{2+} (pH 9): BSA and Cu^{2+} complex present at pH 9 solution)

3.3. Stability of BSA-CuNPs

The instability of CuNPs by oxidation in ambient conditions is a widely recognized issue [9]. Accordingly, the physical and photothermal stability of the BSA-CuNPs was further examined, and the data are summarized in Fig. 4. While keeping the BSA-CuNPs suspension in a 4 °C refrigerator, the wine red color gradually diminished during the 5 days of observation (Fig. 5A). Consistently, the UV-VIS absorbance spectra also showed a gradual reduction in the absorbance (specifically at 400–600 nm region) from Day 1–5 (Fig. 5B). Based on the yellowish color of the dispersion, the oxidized product appeared to be Cu_2O [48]. Despite the oxidation of the CuNPs, notably, the average particle size and the photothermal activity of the BSA-CuNPs did not significantly change during the 5 days of observation (Fig. 5C and D). These results suggest that, consistent with the previous reports of the Cu_2O NPs, the oxidized CuNPs may retain similar particle size and photothermal conversion efficiency to the CuNPs [13].

3.4. Cellular analysis of the cytotoxicity and photothermal activity of BSA-CuNPs

There is growing evidence regarding various bioactivities of the CuNPs, such as anti-microbial, anti-viral, and anticancer activity [31]. Regarding specifically the anticancer activity of the CuNPs, the BSA-CuNPs are known to induce apoptosis by causing oxidative stress on the DNA and mitochondria [49]. The anticancer effects of the BSA-CuNPs were not limited to specific cancer cells but were commonly found in various cancer cells [50].

In the present study, the anticancer activity of BSA-CuNPs was verified using 3 different cancer cell lines (U87 MG, A431, and B16F10). The cytotoxicity results of $CuSO_4$ and BSA-CuNPs are shown in Fig. 6A–C. To all the tested cell lines, both $CuSO_4$ and BSA-CuNPs elicited concentration-dependent cytotoxicity with average IC_{50} values of 36.8 *vs*. 31.6 μgCu/mL (U87 MG), 26.7 *vs*. 10.7 μgCu/mL (A431), and 22.5 *vs*. 9.9 μgCu/mL (B16F10), respectively. The range of the IC_{50} values was in relatively good accordance with previous reports on the IC_{50} values of the Cu-related NPs [31,50,51]. These results, in the one hand, confirm the great anticancer activity of the BSA-CuNPs; yet, on the other hand, these findings highlight possible toxicity concerns. According to a review by Ameh et al., toxicity could be induced by both the CuNPs and the dissolved Cu^{2+} [51]. Once the CuNPs (or Cu^{2+}) internalize the cells, they will likely interact with the organelles, such as mitochondria, and generate reactive oxygen species, thereby leading to DNA cytotoxicity [51]. In addition, they could also induce covalent modification of cellular molecules that could further cause oxidative stress [51]. Hence, further research may be necessary to develop strategies for efficient and safe delivery of CuNPs to the tumor.

When the photothermal cytotoxicity by BSA-CuNPs was evaluated on B16F10 cells, significantly higher cytotoxicity levels were observed from the BSA-CuNPs-treated cells irradiated with the laser than non-laser treated cells (Fig. 6D). Of note, the cells exposed to higher medium temperature by irradiation with a greater power of a laser induced higher levels of cytotoxicity (average cell viability: 67.8%, 23.8%, 8.4%, 7.9% for BSA-CuNPs, BSA-CuNPs+1W, BSA-CuNPs+1.2W, BSA-CuNPs+1.3W, respectively). In sharp contrast,

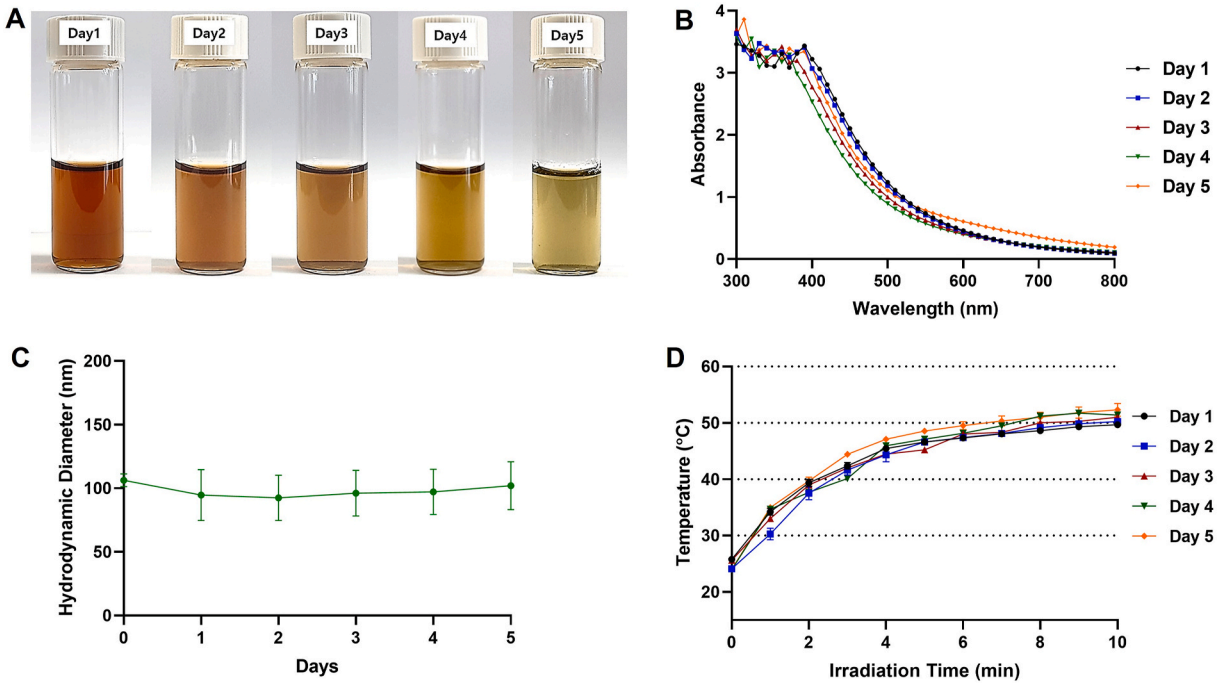

Fig. 5. Inter-day stability of BSA-CuNPs for 5 consecutive days. (A) Optical image change of BSA-CuNPs. (B) The UV-VIS spectrum change of BSA-CuNPs. (C) Hydrodynamic size change of BSA-CuNPs. (D) Light-to-heat conversion efficiency change of BSA-CuNPs. (BSA-CuNPs: bovine serum albumin-coated copper nanoparticles, UV-VIS: ultraviolet–visible)

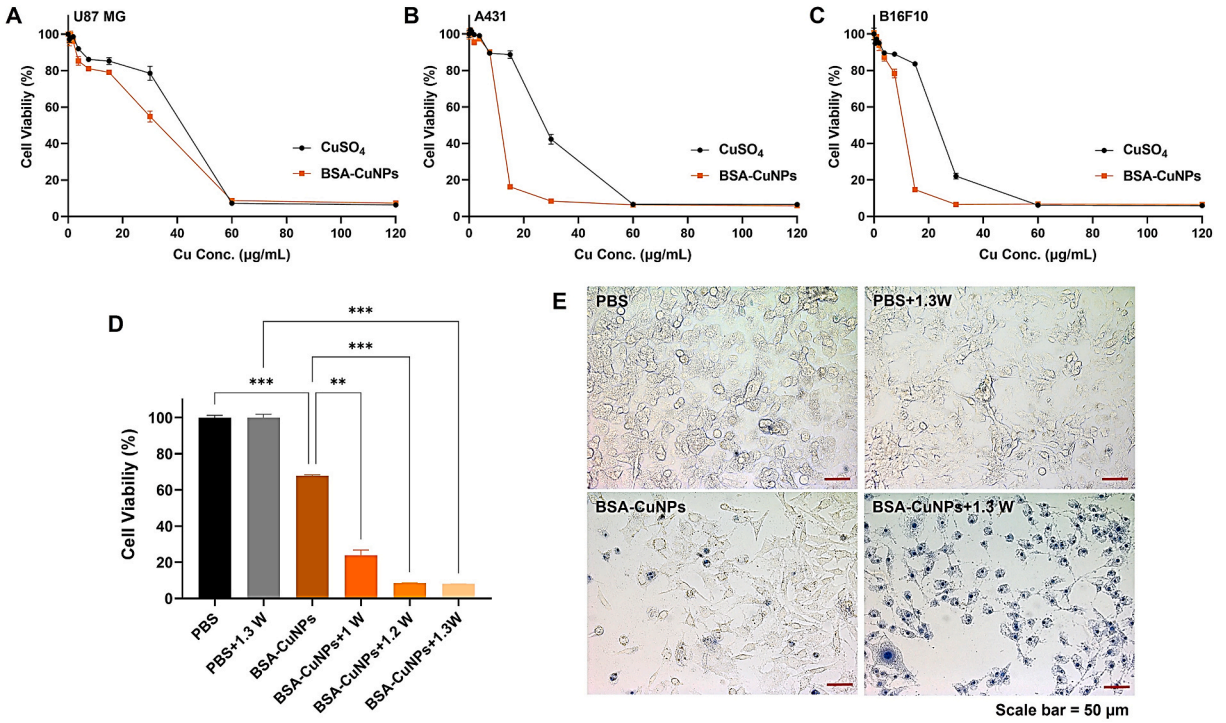

Fig. 6. Anti-cancer activity of BSA-CuNPs. Cytotoxicity profiles of BSA-CuNPs on (A) U87 MG human glioblastoma, (B) A431 human epidermoid squamous carcinoma, and (C) B16F10 murine melanoma cells. The cells were incubated in varying concentrations (0–120 μgCu/mL) of BSA-CuNPs (or $CuSO_4$) and, after 48 h of incubation, the cell viability was measured using the WST-1 assay. (D) Photothermal effects on B16F10 melanoma cells. The viability profiles of BSA-CuNPs-treated cells with laser irradiation (at 1, 1.2, and 1.3 W). The laser powers (1, 1.2, and 1.3 W) were selected to induce the highest medium temperatures of 40, 45, and 50 °C, respectively. The cell viability was measured with the WST-1 assay. (E) Microscopic images of the photothermal-treated cells (× 20 objectives). Dead cells were visualized by the treatment of trypan blue. Statistically significant differences among different groups were tested using 1-way ANOVA (adopting Tukey's multiple comparison test as the post hoc test) with Prism software (GraphPad). $^{**}p < 0.01$ and $^{***}p < 0.001$. (BSA-CuNPs: bovine serum albumin-coated copper nanoparticles and $CuSO_4$: $CuSO_4{\cdot}5H_2O$). (For interpretation of the references to color in this figure legend, the reader is referred to the Web version of this article.)

the control cells irradiated with the 1.3 W laser power showed little cytotoxicity. The microscopic images of the cells showed consistent results with the WST-1 assay data (Fig. 6E). As compared with the control groups, most cells treated with BSA-CuNPs and 1.3 W laser were found dead. Overall, considering the high anticancer activity of BSA-CuNPs and, furthermore, its applicability for PTT, our results confirmed that the BSA-CuNPs possess a great potential to become an effective drug candidate for the treatment of cancer.

3.5. MTD and PK profiles

For evaluation of the biotoxicity of BSA-CuNPs, an MTD study was conducted. The MTD was defined as the maximum bolus dose administered to non-tumor-bearing mice without causing death within 24 h post-administration. Unfortunately, above 32 mgCu/kg, all the tested mice died within 24 h after sample injection. However, there was no death below 16 mgCu/kg, and none of the tested mice showed severe toxicity symptoms. Therefore, the MTD for BSA-CuNPs was estimated to be 16 mgCu/kg.

The PK profiles of BSA-CuNPs were determined in C57BL/6 mice. The plasma concentration-versus-time profile is shown in Fig. 7. Based on the non-compartmental analysis, the calculated plasma half-life was 1.98 h. In addition, the AUC and MRT were 769 μg h/mL and 2.7 h, respectively. These results suggested that, without further modification, the plasma half-life of the BSA-CuNPs might be sufficient to ensure the accumulation of the particles in the tumor region.

4. Conclusions

In the present study, BSA-CuNPs were synthesized by a simple 2-step process that included the stable complex formation of Cu^{2+} with BSA and, subsequently, the reduction of the Cu^{2+} in ambient conditions. The successful preparation of the CuNPs was confirmed by a series of physical characterization, including TEM-EDS, SEM, DSC, XRD, FT-IR, and UV-VIS analyses. The CuNPs possessed superior photothermal activity over the Cu^{2+} and BSA/Cu^{2+} complex. The CuNPs, by themselves, showed significant cytotoxicity on the tested cancer cell lines; however, even higher anticancer effects were achieved with laser treatment. It was found that the photothermal activity could be retained for 5 days in storage conditions. Finally, the preliminary animal study results revealed that it is

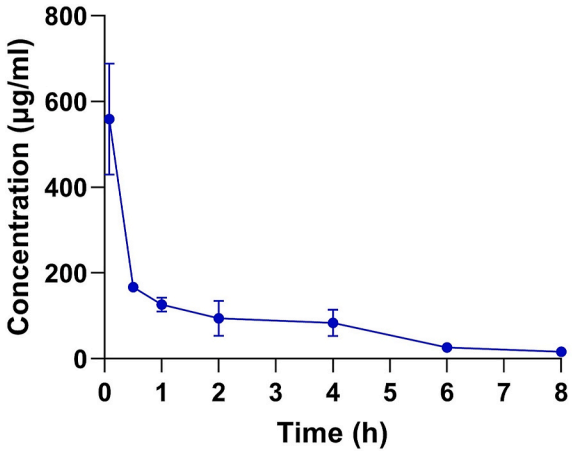

Fig. 7. Plasma concentration-versus-time profiles of BSA-CuNPs after intrvaneous bolus injection to C57BL/6 mice. (BSA-CuNPs: bovine serum albumin-coated copper nanoparticles)

potentially safe to administer the BSA-CuNPs up to 16 mgCu/kg, and the BSA-CuNPs possess a relatively long plasma half-life of 1.98 h. Taken together, our results demonstrated that BSA-CuNPs could potentially serve as an effective PTT agent for cancer therapy.

Author contribution statement

Reeju Amatya; Donghee Lee: Performed the experiments; Analyzed and interpreted the data; Wrote the manuscript.

Marium Sultana: Performed the experiments; Contributed reagents, materials, analysis tools or data.

Kyoung Ah Min: Conceived and designed the experiments; Analyzed and interpreted the data; Contributed reagents, materials, analysis tools or data; Wrote the manuscript.

Meong Cheol Shin: Conceived and designed the experiments; Performed the experiments; Analyzed and interpreted the data; Wrote the manuscript.

Data availability statement

Data included in article/supp. material/referenced in article.

Funding statement

This work was financially supported by the National Research Foundation of Korea (NRF) grant funded by the Ministry of Education, Science and Technology (NRF-2018R1D1A1A02047809 to M.C. Shin, and NRF-2018R1D1A1B07048818 to K.A. Min) and funded by the Korean government (MSIT; Ministry of Science and ICT) (NRF-2021R1F1A1058214 to M.C. Shin, and NRF-2021R1F1A1064206 to K.A. Min). This study was also supported by grants from the Basic Science Research Program through the National Research Foundation of Korea (No. RS-2023-00219399) to M.C. Shin.

Ethics statements

Studies involving animal subjects

Regarding the use of animals, the Gyeongsang National University Institutional Animal Care and Use committee reviewed and approved the animal research (*GNU-220519-M0048-01*). This animal study was carried out following the National Institute of Health Guidelines on the Use of Laboratory Animals and protocol approved by the university committee.

Studies involving human subjects

No human studies were involved in this research.

Additional information

No additional information available for this paper.

Declaration of competing interest

The authors declare that they have no known competing financial interests or personal relationships that could have appeared to influence the work reported in this paper.

Acknowledgements

We thank the National Research Foundation of Korea (NRF) for financially supporting this research.

Appendix A. Supplementary data

Supplementary data related to this article can be found at https://doi.org/10.1016/j.heliyon.2023.e17732.

References

[1] G. Liao, F. He, Q. Li, L. Zhong, R. Zhao, H. Che, et al., Emerging graphitic carbon nitride-based materials for biomedical applications, Prog. Mater. Sci. 112 (2020), 100666, https://doi.org/10.1016/j.pmatsci.2020.100666.
[2] G. Liao, L. Zhang, C. Li, S.-Y. Liu, B. Fang, H. Yang, Emerging carbon-supported single-atom catalysts for biomedical applications, Matter 5 (10) (2022) 3341–3374, https://doi.org/10.1016/j.matt.2022.07.031.
[3] R. Amatya, S. Hwang, T. Park, K.A. Min, M.C. Shin, In vitro and in Vivo evaluation of PEGylated starch-coated iron oxide nanoparticles for enhanced photothermal cancer therapy, Pharmaceutics 13 (6) (2021) 871, https://doi.org/10.3390/pharmaceutics13060871.
[4] R. Amatya, D. Kim, K.A. Min, M.C. Shin, Iron oxide nanoparticles-loaded hydrogels for effective topical photothermal treatment of skin cancer, J. Pharm. Investig. 52 (6) (2022) 775–785, https://doi.org/10.1007/s40005-022-00593-9.
[5] Y. Zou, F. Sun, C. Liu, C. Yu, M. Zhang, Q. He, et al., A novel nanotheranostic agent for dual-mode imaging-guided cancer therapy based on europium complexes-grafted-oxidative dopamine, Chem. Eng. J. 357 (2019) 237–247, https://doi.org/10.1016/j.cej.2018.09.139.
[6] S. Liang, G. Liao, W. Zhu, L. Zhang, Manganese-based hollow nanoplatforms for MR imaging-guided cancer therapies, Biomater. Res. 26 (1) (2022) 32, https://doi.org/10.1186/s40824-022-00275-5.
[7] Y. Zou, H. Jin, F. Sun, X. Dai, Z. Xu, S. Yang, et al., Design and synthesis of a lead sulfide based nanotheranostic agent for computer tomography/magnetic resonance dual-mode-bioimaging-guided photothermal therapy, ACS Appl. Nano Mater. 1 (5) (2018) 2294–2305, https://doi.org/10.1021/acsanm.8b00359.
[8] A. Sharma, A.K. Goyal, G. Rath, Recent advances in metal nanoparticles in cancer therapy, J. Drug Target. 26 (8) (2018) 617–632, https://doi.org/10.1080/1061186X.2017.1400553.
[9] M.B. Gawande, A. Goswami, F.-X. Felpin, T. Asefa, X. Huang, R. Silva, et al., Cu and Cu-based nanoparticles: synthesis and applications in catalysis, Chem. Rev. 116 (6) (2016) 3722–3811, https://doi.org/10.1021/acs.chemrev.5b00482.
[10] H.S. Tuli, R. Joshi, G. Kaur, V.K. Garg, K. Sak, M. Varol, et al., Metal nanoparticles in cancer: from synthesis and metabolism to cellular interactions, J. Nanostruct. Chem. 13 (3) (2023) 321–348, https://doi.org/10.1007/s40097-022-00504-2.
[11] Y. Liu, J. Wu, Y. Jin, W. Zhen, Y. Wang, J. Liu, et al., Copper (I) phosphide nanocrystals for in situ self-generation magnetic resonance imaging-guided photothermal-enhanced chemodynamic synergetic therapy resisting deep-seated tumor, Adv. Funct. Mater. 29 (50) (2019), 1904678, https://doi.org/10.1002/adfm.201904678.
[12] L. Dong, K. Li, D. Wen, Y. Lu, K. Du, M. Zhang, et al., A highly active (102) surface-induced rapid degradation of a CuS nanotheranostic platform for in situ T 1-weighted magnetic resonance imaging-guided synergistic therapy, Nanoscale 11 (27) (2019) 12853–12857, https://doi.org/10.1039/C9NR03830B.
[13] X. Gao, P. Zhang, K. Du, M. Zhang, D. Wen, Y. Lu, et al., Near-infrared-light-responsive copper oxide nanoparticles as efficient theranostic nanoagents for photothermal tumor ablation, ACS Appl. Bio Mater. 4 (6) (2021) 5266–5275, https://doi.org/10.1021/acsabm.1c00410.
[14] Y.-W. Tai, Y.-C. Chiu, P.-T. Wu, J. Yu, Y.-C. Chin, S.-P. Wu, et al., Degradable NIR-PTT nanoagents with a potential Cu@ Cu2O@ Polymer structure, ACS Appl. Mater. Interfaces 10 (6) (2018) 5161–5174, https://doi.org/10.1021/acsami.7b15109.
[15] M. Zhang, Y. Zou, Y. Zhong, G. Liao, C. Yu, Z. Xu, Polydopamine-based tumor-targeted multifunctional reagents for computer tomography/fluorescence dual-mode bioimaging-guided photothermal therapy, ACS Appl. Bio Mater. 2 (2) (2019) 630–637, https://doi.org/10.1021/acsabm.8b00797.
[16] M. Kim, J.H. Lee, J.M. Nam, Plasmonic photothermal nanoparticles for biomedical applications, Adv. Sci. 6 (17) (2019), 1900471, https://doi.org/10.1002/advs.201900471.
[17] Y.-j. Hou, X.-x. Yang, R.-q. Liu, D. Zhao, C.-x. Guo, A.-c. Zhu, et al., Pathological mechanism of photodynamic therapy and photothermal therapy based on nanoparticles, Int. J. Nanomed. 15 (2020) 6827, https://doi.org/10.2147/IJN.S269321.
[18] L. Zhao, Y. Liu, R. Chang, R. Xing, X. Yan, Supramolecular photothermal nanomaterials as an emerging paradigm toward precision cancer therapy, Adv. Funct. Mater. 29 (4) (2019), 1806877, https://doi.org/10.1002/adfm.201806877.
[19] Z. Qin, M. Qiu, Q. Zhang, S. Yang, G. Liao, Z. Xiong, et al., Development of copper vacancy defects in a silver-doped CuS nanoplatform for high-efficiency photothermal–chemodynamic synergistic antitumor therapy, J. Mater. Chem. B 9 (42) (2021) 8882–8896, https://doi.org/10.1039/D1TB01629F.
[20] Z. Mo, M. Qiu, K. Zhao, H. Hu, Q. Xu, J. Cao, et al., Multifunctional phototheranostic nanoplatform based on polydopamine-manganese dioxide-IR780 iodide for effective magnetic resonance imaging-guided synergistic photodynamic/photothermal therapy, J. Colloid Interface Sci. 611 (2022) 193–204, https://doi.org/10.1016/j.jcis.2021.12.071.
[21] Z. Mo, X. Pan, X. Pan, L. Ye, H. Hu, Q. Xu, et al., MOF (Fe)-derived composites as a unique nanoplatform for chemo-photodynamic tumor therapy, J. Mater. Chem. B 10 (42) (2022) 8760–8770, https://doi.org/10.1039/D2TB01691E.
[22] Z. Mo, Q. Li, K. Zhao, Q. Xu, H. Hu, X. Chen, et al., A nanoarchitectonic approach enables triple modal synergistic therapies to enhance antitumor effects, ACS Appl. Mater. Interfaces 14 (8) (2022) 10001–10014, https://doi.org/10.1021/acsami.1c20416.
[23] J. Qin, X. Wang, G. Fan, Y. Lv, J. Ma, Recent advances in nanodrug delivery System for tumor combination treatment based on photothermal therapy, Adv. Therapeutics 6 (3) (2023), 2200218, https://doi.org/10.1002/adtp.202200218.
[24] R. Kumar, K. Mondal, P.K. Panda, A. Kaushik, R. Abolhassani, R. Ahuja, et al., Core–shell nanostructures: perspectives towards drug delivery applications, J. Mater. Chem. B 8 (39) (2020) 8992–9027, https://doi.org/10.1039/D0TB01559H.
[25] T. Park, S. Lee, R. Amatya, H. Cheong, C. Moon, H.D. Kwak, et al., ICG-loaded pegylated BSA-silver nanoparticles for effective photothermal cancer therapy, Int. J. Nanomed. 15 (2020) 5459, https://doi.org/10.2147/IJN.S255874.
[26] D. Kim, R. Amatya, S. Hwang, S. Lee, K.A. Min, M.C. Shin, BSA-silver nanoparticles: a potential multimodal therapeutics for conventional and photothermal treatment of skin cancer, Pharmaceutics 13 (4) (2021) 575, https://doi.org/10.3390/pharmaceutics13040575.
[27] J. Mariam, S. Sivakami, P.M. Dongre, Albumin corona on nanoparticles–a strategic approach in drug delivery, Drug Deliv. 23 (8) (2016) 2668–2676, https://doi.org/10.3109/10717544.2015.1048488.

[28] H.A. Alhazmi, W. Ahsan, A.M. Ibrahim, R.A.Y. Khubrani, Z.A.A. Haddadi, A.Y.F. Safhi, et al., Investigation of bovine serum albumin aggregation upon exposure to silver (I) and copper (II) metal ions using Zetasizer, Open. Chem. 19 (1) (2021) 987–997, https://doi.org/10.1515/chem-2021-0089.
[29] N. Singh, D. Pagariya, S. Jain, S. Naik, N. Kishore, Interaction of copper (II) complexes by bovine serum albumin: spectroscopic and calorimetric insights, J. Biomol. Struct. Dyn. 36 (9) (2018) 2449–2462, https://doi.org/10.1080/07391102.2017.1355848.
[30] B. Khodashenas, H.R. Ghorbani, Synthesis of copper nanoparticles: an overview of the various methods, Kor. J. Chem. Eng. 31 (2014) 1105–1109, https://doi.org/10.1007/s11814-014-0127-y.
[31] P. Aj, J. Dr, S. Ss, Pyrimidine derivative schiff base ligand stabilized copper and nickel nanoparticles by two step Phase transfer method; in vitro anticancer, antioxidant, anti-microbial and DNA interactions, J. Fluorescence 30 (3) (2020) 471–482, https://doi.org/10.1007/s10895-020-02510-5.
[32] P. Adwin Jose, M. Sankarganesh, J. Dhaveethu Raja, G.S. Senthilkumar, R. Nandini Asha, S.J. Raja, et al., Bio-inspired nickel nanoparticles of pyrimidine-Schiff base: in vitro anticancer, BSA and DNA interactions, molecular docking and antioxidant studies, J. Biomol. Struct. Dyn. 40 (21) (2022) 10715–10729, https://doi.org/10.1080/07391102.2021.1947382.
[33] R.N. Asha, M. Sankarganesh, N. Bhuvanesh, B.R.D. Nayagam, Synthesis, structural, spectral, antidiabetic, DNA interactions and molecular docking investigations of a piperidine derivative, J. Mol. Struct. 1250 (2022), 131692, https://doi.org/10.1016/j.molstruc.2021.131692.
[34] P.A. Jose, M. Sankarganesh, J.D. Raja, A. Sakthivel, J. Annaraj, S. Jeyaveeramadhavi, et al., Spectrophotometric and fluorometric detection of DNA/BSA interaction, antimicrobial, anticancer, antioxidant and catalytic activities of biologically active methoxy substituted pyrimidine-ligand capped copper nanoparticles, Spectrochim. Acta Mol. Biomol. Spectrosc. 267 (2022), 120454, https://doi.org/10.1016/j.saa.2021.120454.
[35] J. Jeevitha Rani, A. Mary Imelda Jayaseeli, M. Sankarganesh, R. Nandini Asha, Bovine serum albumin interaction, molecular docking, anticancer and antimicrobial activities of Co (II) Schiff base complex derived from Nophen ligand, J. Biomol. Struct. Dyn. 41 (5) (2023) 1895–1903, https://doi.org/10.1080/07391102.2022.2026249.
[36] S. Gurusamy, R.N. Asha, M. Sankarganesh, T.C. Jeyakumar, A. Mathavan, Vanillin based colorimetric and fluorometric chemosensor for detection of Cu (II) ion: DFT calculation, DNA/BSA interaction and molecular docking studies, Inorg. Chem. Commun. 143 (2022), 109716, https://doi.org/10.1016/j.inoche.2022.109716.
[37] G.S. Senthilkumar, M. Sankarganesh, J. Dhaveethu Raja, A. Sakthivel, R. Vijay Solomon, L. Mitu, Novel metal (II) complexes with pyrimidine derivative ligand: synthesis, multi-spectroscopic, DNA binding/cleavage, molecular docking with DNA/BSA, and antimicrobial studies, Monatshefte für Chemie-Chem. Monthly 152 (2021) 251–261, https://doi.org/10.1007/s00706-021-02737-3.
[38] M. Sankarganesh, P.R. Adwin Jose, J. Dhaveethu Raja, R. Vijay Solomon, C. Dorothy Sheela, S. Gurusamy, Bioactive platinum complex of ligand bearing pyrimidine skeleton: DNA/BSA binding, molecular docking, anticancer, antioxidant and antimicrobial activities, J. Biomol. Struct. Dyn. 40 (15) (2022) 6683–6696, https://doi.org/10.1080/07391102.2021.1889667.
[39] S. Gurusamy, M. Sankarganesh, R. Nandini Asha, A. Mathavan, Biologically active oxovanadium (IV) Schiff base metal complex: antibacterial, antioxidant, biomolecular interaction and molecular docking studies, J. Biomol. Struct. Dyn. 41 (2) (2023) 599–610, https://doi.org/10.1080/07391102.2021.2009916.
[40] Q.-m. Liu, T. Yasunami, K. Kuruda, M. Okido, Preparation of Cu nanoparticles with ascorbic acid by aqueous solution reduction method, Trans. Nonferrous Metals Soc. China 22 (9) (2012) 2198–2203, https://doi.org/10.1016/S1003-6326(11)61449-0.
[41] J. Masuoka, P. Saltman, Zinc (II) and copper (II) binding to serum albumin. A comparative study of dog, bovine, and human albumin, J. Biol. Chem. 269 (41) (1994) 25557–25561, https://doi.org/10.1016/S0021-9258(18)47285-7.
[42] F. Hadinejad, M. Jahanshahi, H. Morad, Microwave-assisted and ultrasonic phyto-synthesis of copper nanoparticles: a comparison study, Nano Biomed. Eng. 13 (1) (2021) 6–19, https://doi.org/10.5101/nbe.v13i1.p6-19.
[43] E.M. Derun, N. Tugrul, F.T. Senberber, A.S. Kipcak, S. Piskin, The optimization of copper sulfate and tincalconite molar ratios on the hydrothermal synthesis of copper borates, Int. J. Chem. Mol. Eng. 8 (10) (2014) 1152–1156, https://doi.org/10.5281/zenodo.1096563.
[44] J. Grdadolnik, Y. Maréchal, Bovine serum albumin observed by infrared spectrometry. I. Methodology, structural investigation, and water uptake, Biopolym. Orig. Res. Biomol. 62 (1) (2001) 40–53, https://doi.org/10.1002/1097-0282(2001)62:1<40::AID-BIP60>3.0.CO;2-C.
[45] Y.-T. Chen, P.-H. Lee, P.-T. Shen, J. Launer, R. Oketani, K.-Y. Li, et al., Study of nonlinear plasmonic scattering in metallic nanoparticles, ACS Photonics 3 (8) (2016) 1432–1439, https://doi.org/10.1021/acsphotonics.6b00025.
[46] J.A. Jiménez, Excitation-dependent enhancement and quenching of the 1.54 μm emission from Er3+ ions in dichroic Cu nanocomposite glass, Solid State Commun. 321 (2020), 114046, https://doi.org/10.1016/j.ssc.2020.114046.
[47] J. Lian, J. Fu, Pioglitazone for NAFLD patients with prediabetes or type 2 diabetes mellitus: a meta-analysis, Front. Endocrinol. 12 (2021), 615409, https://doi.org/10.3389/fendo.2021.615409.
[48] A.V. Markin, N.E. Markina, Experimenting with plasmonic copper nanoparticles to demonstrate color changes and reactivity at the nanoscale, J. Chem. Educ. 96 (7) (2019) 1438–1442, https://doi.org/10.1021/acs.jchemed.8b01050.
[49] M. Maliki, I.H. Ifijen, E.U. Ikhuoria, E.M. Jonathan, G.E. Onaiwu, U.D. Archibong, et al., Copper nanoparticles and their oxides: optical, anticancer and antibacterial properties, Int. Nano Lett. 12 (2022) 379–398, https://doi.org/10.1007/s40089-022-00380-2.
[50] E.G. Halevas, A.A. Pantazaki, Copper nanoparticles as therapeutic anticancer agents, Nanomed. Nanotechnol. J. 2 (1) (2018) 119–139.
[51] T. Ameh, C.M. Sayes, The potential exposure and hazards of copper nanoparticles: a review, Environ. Toxicol. Pharmacol. 71 (2019), 103220, https://doi.org/10.1016/j.etap.2019.103220.